

Technical Activities Execution with a TiltRotor UAS employing Explicit Model Predictive Control

Christos Papachristos* Kostas Alexis** Anthony Tzes***

* *Electrical and Computer Engineering Department, University of Patras, Rio 26500 Greece (email: papachric@ece.upatras.gr)*

** *Autonomous Systems Lab, ETH-Zurich, Zurich 8092 Switzerland (email: konstantinos.alexis@mavt.ethz.ch)*

*** *Electrical and Computer Engineering Department, University of Patras, Rio 26500 Greece (email: tzes@ece.upatras.gr)*

Abstract: An innovative application field for Unmanned Aerial Systems (UASs) is the subject of this paper. The aerial robotic execution of technical activities based on autonomous aerial platforms poses important challenges, as realistic industrial activities are physically demanding. Typical environment-modifying tasks, such as surface grinding, require the exertion of significant forces in order to be successfully executed. For such purposes, the exploitation of thrust-vectoring actuation is proposed, and a methodology for achieving longitudinal force exertion while retaining safe operation is developed, relying on the platform's exceptional actuation features, a piecewise-affine representation of the system modes, and an explicit model predictive control scheme. The experimental demonstration of the proposed strategy is conducted utilizing a compound UAS, consisting of a high-end tilt-rotor vehicle, mounted with an end-effector which carries a motorized tool customized for surface grinding tasks.

1. INTRODUCTION

As Unmanned Aerial Systems (UASs) are technologically maturing, novel research fields have sprung forth, aiming to extend the capabilities inherent to their aerial nature to address applications typically regarded as human operator or ground robot-oriented. Following –and benefiting from– a wide basis of achievements (Alexis et al. [2012], Alexis et al. [2010], Goga and Boek. [2013]), while exceeding the role of UASs as eyes-in-the-sky, current research directions include grasping and carrying small objects (Mellinger et al. [2011], Thomas et al. [2013], Pounds et al. [2011], Korpela et al. [2012]), cooperative object transportation and manipulation (Mellinger et al. [2013], Manubens et al. [2013]), and surface inspection through contact (Darivianakis et al. [2014], Alexis et al. [2013], Marconi and Naldi [2012]). Attempting to make one more leap forward, an aspiring UAS is envisioned, one that can actively interact with a rigid environment and produce a drastic change upon it. This surpasses the current applications of aerial robotic manipulation, and targets the field of industrial-style operations such as drilling, bolting, cutting and grinding.

In this process, the human technician paradigm is considered, i.e. combining body motion in order to forcefully push against the environment while conducting precision activities with the hands. Forceful interaction tasks, such as surface rust-grinding, can be performed very efficiently with robots on the ground (Koveos et al. [2012]). The transportation of this paradigm in the air requires: a) a stable platform capable of exerting a large force in the longitudinal direction, and b) an end-effector tool to perform

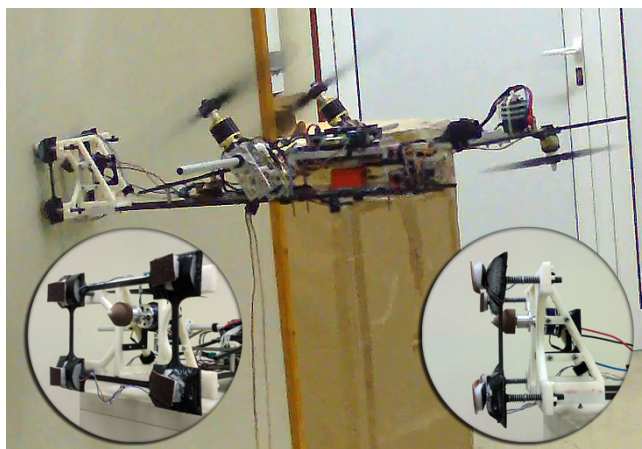


Fig. 1. The Tri-TiltRotor UAS in Technical Activity Execution. Detail: The Motorized-Tool End-Effector

the required operation. To this end, the exploitation of the direct thrust-vectoring capability of tiltrotor Unmanned Aerial Vehicle (UAV) platforms gains an innovative aspect: via rotor-tilting a controlled forward-exerted force is generated, while the UAV retains its attitude control authority and ensures stable regulation around the hovering pose. Hence, the tool/end-effector is reduced to a snap-on, mostly rigid-body design, seamlessly integrated into the envisioned UAS. In completion of the proposed concept, an explicit Model Predictive Control framework is employed, relying on a Piece-Wise Affine system model representation. This scheme provides control optimality, respects the system state and input constraints, while

also ensuring stable transition among the system's free-flight/physical-interaction modes.

The article is structured as follows: In Section 2 the experimental setup and in Section 3 the system model are elaborated. In Section 4 the control synthesis and in Section 5 experimental technical task execution results are presented. The article is concluded in Section 6.

2. EXPERIMENTAL SETUP

The operational scenario is illustrated in Figure 2. Its sub-components are: *i*) the UPAT Tri-TiltRotor (Papachristos et al. [2013], Papachristos et al. [2012], Papachristos et al. [2011]), *ii*) an end-effector frame equipped with a motorized tool, and *c*) the rigid environment.

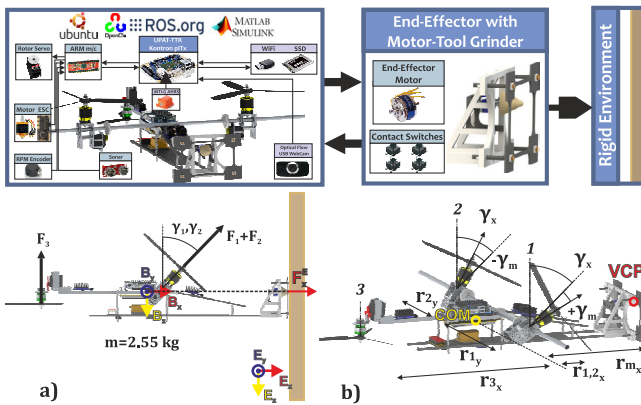


Fig. 2. The TiltRotor - Motor-Tool End-Effector UAS

The end-effector frame mostly consists of 3D-printed parts: a rigid base (white) and a 4-contact-point surface (black), with 4 springs allowing relative compressing motion. The grinder-tool nose comes into contact with the environment surface only after the springs have been compressed by a certain length, and thus a certain forward-force is being applied by the UAV. The magnitude of this force threshold is such, that the friction at the 4 contact points does not allow lateral or vertical sliding. Further spring compression requires a higher force, and occurs as the grinder-tool progressively removes surface material. The compliant end-effector additionally absorbs part of the impact energy during docking. The 4-contact-point surface is equipped with tactile switches, enabling contact feedback. Each spring is separately compressible, allowing a certain 2-DoF rotational freedom of the UAS w.r.t the environment surface.

The motorized tool is mounted on the end-effector base via a different set of fully compressed springs. These do not allow the tool to retreat while grinding, but they can be flexed and allow it to side-slip in case a very hard point in the internal structure is reached (solid metal while grinding rust layers, wood knob, etc.), relieving the built-up energy and locally damping the introduced vibrations.

The UPAT-TTR platform is equipped with onboard sensors and an autonomous state-estimation scheme, enabling the execution of the proposed scenario. The envisioned operation clearly demonstrates the utility of the proposed UAS: grinding a rigid surface (e.g. in order to clear an

outer layer hole to perform structural measurements), requires not only the proper tool, but also a stable platform to forcefully press it against the surface, while retaining operational safety.

3. SYSTEM MODELING FOR CONTROL

The utilized Body-Fixed Frame (BFF) $\mathbf{B} = \{B_x, B_y, B_z\}$, and North-East-Down (NED) Local Tangential Plane (LTP) $\mathbf{E} = \{E_x, E_y, E_z\}$ are depicted in Figure 2.

Let the states $\Theta = \{\phi, \theta, \psi\}$ and $\mathbf{X} = \{x, y, z\}$ be the LTP-based rotation angles and position vectors respectively, let $i \rightarrow [1, 2, 3]$ mark the right, left and tail rotor, and let $\mathbf{R}_i = \{F_i, \gamma_i\} = \{F_i^0 + \delta F_i, \gamma_i^0 + \delta \gamma_i\}$ mark the thrust force and the rotor-tilt angle of the i -th rotor, forming the baseline system state and actuator input vectors as:

$$\mathbf{X} = [\mathbf{X} \dot{\mathbf{X}} \Theta \dot{\Theta}]^T = [x \ y \ z \ \dot{x} \ \dot{y} \ \dot{z} \ \phi \ \theta \ \psi \ \dot{\phi} \ \dot{\theta} \ \dot{\psi}]^T \quad (1)$$

$$\mathbf{U}_a = [\mathbf{R}_1 \ \mathbf{R}_2 \ \mathbf{R}_3]^T = [F_1 \ \gamma_1 \ F_2 \ \gamma_2 \ F_3 \ \gamma_3]^T \quad (2)$$

Also, m marks the UAS mass, $\mathbf{r}_i = \{r_{i_x}, r_{i_y}, r_{i_z}\}$ mark the BFF-based geometric distance from the COM to the i -th rotor's propeller hub (which are functions of γ_i as described in Papachristos et al. [2012]), and $\mathbf{r}_m = \{r_{m_x}, r_{m_y} = 0, r_{m_z} = 0\}$ mark the BFF-based geometric distance from the Center Of Mass (COM) to the centroid of the end-effector front surface plane, which is mechanically configured to be collinear. Provided the UAS maintains a stable hovering attitude pose $\{\phi \simeq 0, \theta \simeq 0\}$ while docked, the end-effector front centroid can be regarded as a Virtual Contact Point (VCP).

3.1 Steady-State Overview

Let FF mark the Free-Flight system mode, and PA mark the Physical Activity mode wherein the UAS is docked onto the rigid environment surface. Tilting the main rotors by $\gamma_1 \simeq \gamma_2$ achieves longitudinal projection of their thrust, which in the FF -mode can be exploited for navigation, while in the PA -mode it is used for longitudinal force exertion. Figure 2-a depicts how the platform's additional control authority can be employed to achieve vertical forces and pitch moment equilibrium. The rotor thrust offsets are commanded as:

$$[F_1^0 \ F_2^0 \ F_3^0]^T = \left[\frac{c_1 mg}{\cos(\gamma_1)} \ \frac{c_2 mg}{\cos(\gamma_2)} \ c_3 mg \right]^T \quad (3)$$

where c_i are control mixing coefficients (due to the asymmetrical UAS mechanical configuration). This is implementable in the form of a feedforward control scheme and enables the UAS to retain the $\{\phi \simeq 0, \theta \simeq 0\}$ hovering attitude pose in either mode. Furthermore, due to the mechanical collinearity of the VCP with the COM, no additional pitch moment is generated w.r.t the VCP (Papachristos and Tzes. [2013]), and for near-equally $\gamma_1 \simeq \gamma_2$ tilted rotors ($r_{1_x} = r_{2_x} = r_{1,2_x}$), the coefficients are calculated as: $c_1 = c_2 = \frac{r_{3_x}}{2(r_{1,2_x} + r_{3_x})}$, $c_3 = \frac{r_{1,2_x}}{r_{1,2_x} + r_{3_x}}$.

Finally, Figure 2-b exposes the capability to exploit differential thrust vectoring to generate a yaw ψ -moment in the

PA mode. Considering the moment of the longitudinally-projected thrust components $\{F_{1_x}, F_{2_x}\}$ w.r.t the VCP:

$$M_\psi^{VCP} \simeq F_{2_x} r_{2_y} - F_{1_x} r_{1_y} \leq 0 \Rightarrow F_{1_x} \geq F_{2_x}, \quad (4)$$

as $r_{1_y} = r_{2_y}$. The rotors are tilted differentially by $\pm\gamma_m$ such that $\gamma_1 = \gamma_x \pm \gamma_m, \gamma_2 = \gamma_x \mp \gamma_m$, and their thrust offsets are adjusted as per (3) to retain $\{z, \phi\}$ -axes equilibrium w.r.t. the VCP. This concurrent differential thrusting further increases the magnitude of the generated M_ψ^{VCP} moment. Since the end-effector design allows a certain rotational freedom via the separately compressible springs, this principle can be used to control the orientation of the applied force while executing a certain task (e.g. enabling the UAS to side-grind with the motorized grinder).

3.2 Attitude

In the *FF*-mode, along the standard tri-rotor control approach, a virtual input vector $\delta\mathbf{U}_\Theta$ is utilized, such that each input manipulates the moment (with respect to the COM) driving each attitude DoF in a decoupled sense: $\delta\mathbf{U}_\Theta = \{\delta u_\phi, \delta u_\theta, \delta u_\psi\} \rightarrow \delta\mathbf{M}_\Theta = \{\delta M_\phi, \delta M_\theta, \delta M_\psi\}$.

In the *PA* mode the UAS is docked onto the external surface via the end-effector frame, where the objective is the stable regulation around the hovering pose $\{\phi \simeq 0, \theta \simeq 0\}$. Assuming a contact-maintaining longitudinally exerted force, the UAS is regarded as attached at the VCP. For simple attitude regulation purposes, it is considered sufficient to retain a similar decoupled control structure, while the pitch command is allocated collectively to the rotors, as the new center of rotation (the VCP) lies ahead of the main rotors.

The control allocation is summarized by:

$$\delta\mathbf{U}_{a,\Theta}^{[FF/PA]} = \begin{bmatrix} \delta F_{1,\Theta} \\ \delta\gamma_{1,\Theta} \\ \delta F_{2,\Theta} \\ \delta\gamma_{2,\Theta} \\ \delta F_{3,\Theta} \\ \delta\gamma_{3,\Theta} \end{bmatrix} = \begin{bmatrix} -\delta u_\phi + c_1([+/-]\delta u_\theta) \\ 0 \\ \delta u_\phi + c_2([+/-]\delta u_\theta) \\ 0 \\ c_3(-\delta u_\theta) \\ -\delta u_\psi \end{bmatrix}. \quad (5)$$

Finally, it is noted that the tri-tiltrotor platform makes use of the typical underactuated multirotor control approach only in driving its lateral y -axis dynamics, while the x -axis dynamics are fully actuated via the additional rotor-tilting control authority, and the z -axis dynamics are actuated via rotor thrusting. Therefore, in the presented framework, only hovering pitch regulation control is considered.

3.3 Translation

The two distinct modes motivate the use of a PieceWise Affine (PWA) system model representation for control. The translational subsystem dynamics ($\{x, y, z\}$) are considered as decoupled, provided that consistent hovering attitude pose $\{\phi \simeq 0, \theta \simeq 0\}$ regulation is ensured.

The longitudinal dynamics are driven by the collective rotor-tilt angle $\gamma_x = \frac{\gamma_1 + \gamma_2}{2}$, the dynamics of which were identified in the Frequency Domain (Ljung [1999]) with a first-order structure: $\dot{\gamma}_x = -a_\gamma\gamma_x + b_\gamma\dot{\gamma}_x^r$. The x -subsystem is described by the following state-space representations:

$$\dot{\mathbf{x}}_x = [x \dot{x} \gamma_x F_x^E]^T, \quad \mathbf{u}_x = \gamma_x^T \quad (6)$$

$$FF : \dot{\mathbf{x}}_x = \begin{bmatrix} 0 & 1 & 0 & 0 \\ 0 & -d_x^{FF} & g(c_1 + c_2) & 0 \\ 0 & 0 & -a_\gamma & 0 \\ 0 & 0 & 0 & 0 \end{bmatrix} \mathbf{x}_x + \begin{bmatrix} 0 \\ 0 \\ b_\gamma \\ 0 \end{bmatrix} \mathbf{u}_x \quad (7)$$

$$PA : \dot{\mathbf{x}}_x = \begin{bmatrix} 0 & 1 & 0 & 0 \\ 0 & -d_x^{PA} & 0 & 0 \\ 0 & 0 & -a_\gamma & 0 \\ 0 & 0 & 0 & -a_\gamma \end{bmatrix} \mathbf{x}_x + \begin{bmatrix} 0 \\ 0 \\ b_\gamma \\ b_\gamma m g(c_1 + c_2) \end{bmatrix} \mathbf{u}_x \quad (8)$$

where F_x^E is the longitudinal force applied on the environment surface. This additional force-state (estimated as $F_x \simeq (F_1^0 + F_2^0)\sin(\gamma_x)$ when contact feedback via the end-effector tactile switches is detected, while otherwise $F_x^E = 0$) is used in encoding the guard-rules used to switch among the two distinct modes:

$$\mathcal{G}^{FF} : F_x^E \leq 0, \quad \mathcal{G}^{PA} : F_x^E \geq 0. \quad (9)$$

This force-state can also be manipulated in the *PA*-mode, as encoded in (8), in order to achieve exerted-force control for technical activities execution. Finally, d_x^{FF} encodes the effect of a FD-identified damped pole in the *FF*-mode dynamics, and d_x^{PA} is a longitudinal velocity-damping term, mostly determined by the viscous damping coefficient of the springs in the end-effector front surface.

The lateral subsystem and the vertical subsystem in the *FF*-mode are treated as per the usual multirotor approach (Papachristos et al. [2013]). Moreover, as the purpose of the proposed control structure is not to manipulate the UAS position while docked, lateral-and-vertical control are disabled at the *PA*-mode, and contact stiction (ensured by maintaining a minimum longitudinally-exerted force, as elaborated within the consequent Section) is considered adequate to constrain the platform and prevent sliding.

3.4 Technical Discussion: The Directly-Actuated UAS

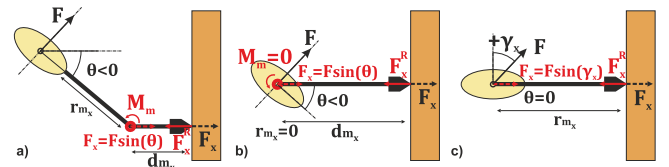


Fig. 3. Technical Analysis of UAS-based Force Exertion Principles

This section discusses the advantages offered by the proposed UAS in a range of tasks that require forceful interaction in order to execute physically-demanding activities. Figure 3-a illustrates the use of an underactuated platform for such purposes. As elaborated in Papachristos et al. [2014], this practice which is based on pitch rotation of the entire UAV body poses safety-related issues: The system's thrust authority is commanded as $F = \frac{m g}{\cos(\theta)}$, in order to generate a longitudinally-exerted force $F_x = F \sin(-\theta)$, and assuming contact stiction, moment calculation with respect to the UAV COM yields:

$$F_x = F \sin(-\theta), \quad F = \frac{m g}{\cos(\theta)} \quad (10)$$

$$M_\theta = (F_x - F_x^R)r_{m_x} \sin(-\theta) = \Delta F_x r_{m_x} \sin(-\theta) \quad (11)$$

$$\frac{\partial M_\theta}{\partial \Delta F_x} = r_{m_x} \sin(-\theta) \quad (12)$$

In (12) it is noted that a sudden force imbalance $\partial\Delta F_x$ (normally expected while executing technical tasks) will cause a ∂M_θ moment disturbance, the effect of which is increased with the pitch angle.

More specifically regarding the execution of technical activities, in order to maintain the end-effector tool normal to the environment surface, a joint is required, upon which a M_m -moment is in effect. Passive joint designs (with deformable elastic components) pose the efficiency-related issue that a constant counteracting moment will be active as the UAV increases the magnitude of its θ -operating angle, while an active-components actuator-driven joint would require a more complex design process.

As indicated by (12), in order to minimize the aforementioned disturbing effects, either the r_{m_x} arm or the θ -operating angle needs to be minimized. Figure 3-b illustrates the first approach, where the underactuated principle is retained: the UAV-body is rotated for longitudinal thrust-force projection, while the end-effector joint is placed near the COM ($r_{m_x} = 0$). The second approach ($\theta = 0$) is depicted in Figure 3-c, where no end-effector joint is required as longitudinal force generation is achieved via the γ_x direct thrust-vectoring feature of a rotor-tilting UAV platform-type.

While both methodologies can provide the control-wise operational safety requirements, the first approach focuses in adding to the end-effector capabilities, while the second is based on the additional authority incorporated in directly-actuated platforms, requiring a reduced-complexity end-effector design. It is eventually noted that the first methodology would prove to be a redundant feature in the FF -mode of an underactuated UAV design, whereas rotor-tilting is a directly exploitable feature in FF -navigation.

4. CONTROL SYNTHESIS

The control scheme of the proposed UAS for technical activities execution is illustrated in Figure 4. It consists of the feedforward steady-state Force/Moment Compensator, and the output feedback-driven Attitude Dynamics Controller and Translational Dynamics Controller.

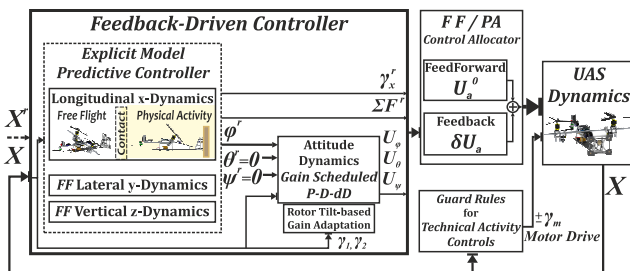


Fig. 4. The TiltRotor - Motor-Tool End-Effector UAS Control Scheme for Technical Activities Execution

For the Force/Moment Compensator implementation, (3) gives the feedforward-manipulated control signals required to maintain hovering force/moment equilibrium at all times. Regarding the Attitude Dynamics Controller, the output feedback-driven Gain-Scheduled Proportional, Derivative, double-Derivative control structure (Papachristos et al. [2013]) is retained for the FF -mode. In the PA -mode, continuous adaptation of the feedback

gains as functions of the rotor-tilt angles γ_i is performed, such that the generated attitude rates remain the same as in the hovering FF -mode for a given attitude state-error vector. Contact feedback via the front tactile switches is used to switch among the θ -control allocations (5).

4.1 Translational Dynamics Controller

The Translational Dynamics Control synthesis consists of a Model Predictive Control (MPC) scheme based on the PWA linearized approximations of the active dynamics at each distinct operational mode. The scheme lies on the foundations of receding horizon control, and provides the important features of control optimality, respect of state and input constraints, global stability for the switching dynamics, while also accounting for the actuation subsystem dynamics (as incorporated in the previously presented models). In the optimal control computation process, a set of state and input constraints are incorporated, in order to ensure a safe flight-envelope:

$$\begin{bmatrix} \mathbf{I}_{3 \times 3} & \mathbf{0}_{3 \times 3} \\ \mathbf{0}_{3 \times 3} & -\mathbf{I}_{3 \times 3} \end{bmatrix} \begin{bmatrix} \dot{x} \\ \gamma \\ \gamma^r \\ \dot{x} \\ \gamma \\ \gamma^r \end{bmatrix} \leq \begin{bmatrix} 1\text{m/s} \\ \pi/4\text{rad} \\ \pi/4\text{rad} \\ 1\text{m/s} \\ \pi/8\text{rad} \\ \pi/8\text{rad} \end{bmatrix} \quad (13)$$

The multiparametric optimization problem is solved using a set of powerful high-end tools (Herceg [2013], Loeferberg [2004]), based on the PWA representation of the longitudinal dynamics, while the same framework is also utilized for the constrained optimal control of the FF -LTI lateral and vertical dynamics (which are not elaborated as they do not consist significant contributions). The quadratic optimality metric is employed over a prediction horizon N , computing the optimal control sequence $\mathcal{U}_v^N = [\mathcal{U}_v(0), \dots, \mathcal{U}_v(N-1)]$ that achieves minimization of the objective function:

$$\begin{aligned} \mathbf{J}(\mathcal{X}_{v,0}, \mathbf{U}_v^N) &= \min_{\mathbf{U}_v^N} \{ \mathcal{X}_{v,N}^T \mathbf{P}_{M \times M} \mathcal{X}_{v,N} + \\ & \quad v \rightarrow [x, y, z] \quad \sum_{k=0}^{N-1} \mathcal{X}_{v,k}^T \mathbf{Q}_{M \times M} \mathcal{X}_{v,k} + \\ & \quad [(9) : \{(7), (8)\}] \quad \mathcal{U}_{v,k}^T \mathbf{R}_{L \times L} \mathcal{U}_{v,k} \\ & \quad [13] \quad \mathcal{X}_{v,N} \in T_v^{set} \end{aligned} \quad (14)$$

where for each v -translational subsystem, $\mathbf{P}_{M \times M} \succeq \mathbf{0}$, $\mathbf{Q}_{M \times M} \succeq \mathbf{0}$, $\mathbf{R}_{L \times L} \succeq \mathbf{0}$ are the weighting matrices of the terminal state, the subsystem states and the manipulated inputs. Finally, T_v^{set} is the LQR-computed terminal set in order to guarantee stability properties (Baotic [2005]).

The previously elaborated qualities of the proposed MPC-scheme come at the cost of computational complexity, as they consist of linear programming optimization problems to be solved at each time-step. The real-time implementation of such control structures therefore depends highly on the on-board processing resources available in order to provide an online-computed solution, resources which may however be encumbered by other significant tasks such as computer-vision for state estimation and localization. One important feature of this scheme is the capability for its offline-computed explicit representation

as a set of state vector-based convex polyhedral regions $\mathcal{P}_v^r = \{\mathcal{X}_v^k | \mathbf{H}_v^r \mathcal{X}_v^k \leq \mathbf{K}_v^r\}$, within which the optimal control action law is expressed in the form of state-feedback gains \mathbf{F}_v^r and affine terms \mathbf{G}_v^r :

$$\mathbf{U}_v^k = \mathbf{F}_v^r \mathcal{X}_v^k + \mathbf{G}_v^r, \quad : \mathcal{X}_v^k \in \mathcal{P}_v^r. \quad (15)$$

This representation of the receding horizon control strategy is made possible by the fact that the solution of such multiparametric optimization problems is in the piecewise affine form (Kvasnica [2009]). Moreover, it is equivalent to the online strategy, as the same state trajectories result in identical control actions, and thus the explicit control solution is characterized by the same stabilizing and optimality properties (Bemporad [2003]). The derivation of the optimal control action for each $v \rightarrow \{x, y, z\}$ -subsystem can therefore be obtained based on the set of $\mathcal{P}_v^r : [\mathbf{H}_v^r, \mathbf{K}_v^r]$ polyhedral constraints and $\mathcal{C}_v^r : [\mathbf{F}_v^r, \mathbf{G}_v^r]$ control coefficients via an extension of the table traversal algorithm (Kvasnica et al. [2010]), presented in Table 1:

Algorithm 1: Extended Table Traversal Algorithm

Data: Regions: H_v^r, K_v^r Region Feedback Coefficients: F_v^r, G_v^r ,
Region Cost Matrices: Q_v^r, f_v^r, g_v^r , Regions Number: N^r ,
Input Cost Matrix: R_v^r , State at Time k : \mathcal{X}_v^k , Previous
Optimal Control Input: \mathcal{U}_v^{k-1}

Result: MPC Optimal Control Input \mathcal{U}_v^k

```

 $J_v^{min} \leftarrow +\infty;$  /* Quadratic Cost Initialization */
 $\mathcal{U}_v^{opt} \leftarrow \mathcal{U}_v^{k-1};$  /* Optimal Input Initialization */
for  $r = 1, \dots, N^r$  do
    if  $H_v^r \mathcal{X}_v^k \leq K_v^r$  then
         $J_v^r \leftarrow \mathcal{X}_v^{kT} Q_v^r \mathcal{X}_v^k + f_v^{rT} \mathcal{X}_v^k + g_v^r;$  /* Region Cost */
         $\mathcal{U}_v^r \leftarrow F_v^r \mathcal{X}_v^k + G_v^r;$  /* Region Control Input */
        if  $J_v^r < J_v^{min}$  then
             $J_v^{min} \leftarrow J_v^r;$ 
             $\mathcal{U}_v^{opt} \leftarrow \mathcal{U}_v^r;$ 
        else if  $J_v^r = J_v^{min}$  then
            if  $\mathcal{U}_v^{rT} R_v^r \mathcal{U}_v^r \leq \mathcal{U}_v^{optT} R_v^r \mathcal{U}_v^{opt}$  then
                 $J_v^{min} \leftarrow J_v^r;$ 
                 $\mathcal{U}_v^{opt} \leftarrow \mathcal{U}_v^r;$ 
            end
        end
    end
end
return  $\mathcal{U}_v^{opt};$ 

```

4.2 Technical Activity Controls

It is noted that this work does not address a specific technical task. Instead it proposes a methodology for aerial robotic technical activity execution by relying on a UAS design equipped with thrust-vectoring capabilities, and a control scheme that achieves the key-features of: efficient navigation in the *FF*-mode, stable *FF* \rightarrow *PA*-transitioning during docking, and externally-applied longitudinal force F_x^E control, while safely operating at the $\{\phi \simeq 0, \theta \simeq 0\}$ hovering attitude pose. The task-specific controls (associated with the demonstrated surface-grinding activity) are incorporated into the control structure only w.r.t. their impact on operational safety. As previously discussed, a minimum forward-exerted force achieving interfacing stiction between the end-effector and the environment surface is considered as a threshold, in

order to ensure that no sliding motion can occur, despite the disturbing effects of the technical activity:

$$\mathcal{G}^0 : F_x^E < F_x^{E,min}, \quad \mathcal{G}^1 : F_x^E \geq F_x^{E,min}, \quad (16)$$

where $\mathcal{G}^0, \mathcal{G}^1$ the guard-rules which determine when the technical activity-related inputs (motor-tool drive, differential rotor thrusting $\pm\gamma_m$) are disabled-or-enabled respectively. The $F_x^{E,min} = 5\text{N}$ was experimentally determined for a test-case slick external surface, which consists a conservative but reliable operational threshold.

5. EXPERIMENTAL STUDIES

The experimental implementation of the proposed UAS, employing the elaborated explicit MPC control synthesis yielded successful technical task execution results. It is important to note that this scheme consists of a unified structure, which efficiently handles: a) free-flight operation, b) surface docking/detaching, and c) controlled forceful interaction for technical activities execution. The Attitude Dynamics Control loops operate at $f_\Theta = 100\text{Hz}$, and the Translational Dynamics Explicit MPC loops are computed for $f_X = 10\text{Hz}$, and a $N = 3$ prediction horizon. For each experimental sequence the following results are provided in the respective order:

a) The longitudinal force reference signal $F_x^{E,ref}$ and the estimated longitudinally-applied force F_x^E . It is highlighted that F_x^E does not represent the forward-projected force, considered active only when contact feedback via the tactile switches is detected, and zero otherwise. The force reference is initially commanded as $F_x^{E,ref} = F_x^{E,min}$, afterwards it varies depending on the required operation, while finally it is commanded as $F_x^{E,ref} = -F_x^{E,min}$ in order to detach the UAS from the environment surface.

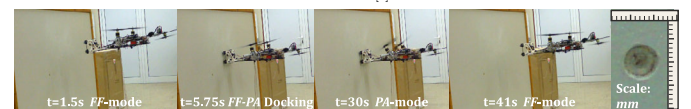
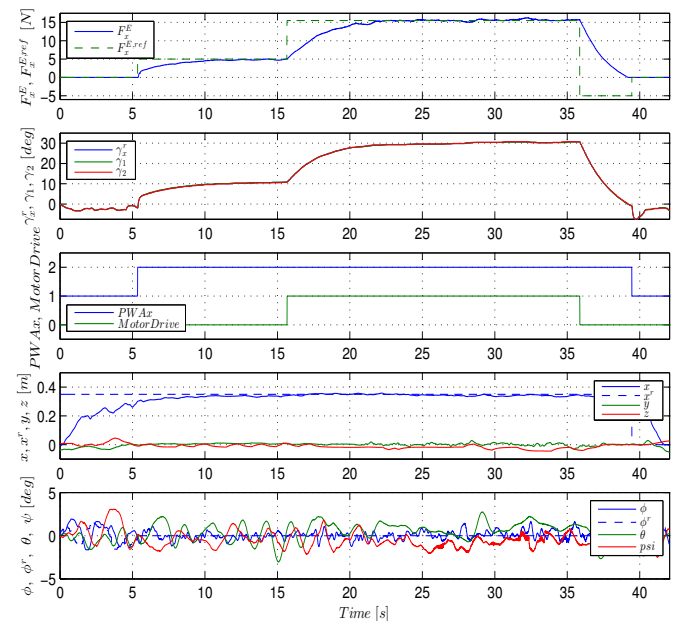


Fig. 5. *FF*-Navigation, Docking, Basic Technical Activity

b) The rotors' distinct tilt angles γ_1, γ_2 , and the collective tilt angle γ_x . It is noted that γ_x is driven by the MPC PWA-based controller in order to navigate in the FF -mode and achieve force control in the PA -mode, while a differential component $\pm\gamma_m$ may be applied when the motorized tool is active to enact a rotating moment while performing grinding as in (4). At the same time roll ϕ -moment static equilibrium is retained, as previously elaborated.

c) The logical signals PWA_x and $MotorDrive$, respectively representing the active longitudinal PWA dynamics at each time instant as driven by (9), and the motorized tool activity which is only allowed to be activated based on the guard rule (16).

d) The UAS's LTP-based $\{x, y, z\}$, marking the evolution of the translational dynamics during the FF , the $FF \rightarrow PA$ docking transition, and the PA phases. A x^r reference signal is used to drive the UAS towards the external surface; this position reference is reset after the $PA \rightarrow FF$ detaching transition, returning the UAS to the origin.

e) The evolution of the UAS's attitude dynamics, depicting the stable regulation around the $\{\phi \simeq 0, \theta \simeq 0\}$ hovering attitude pose, considered as the key-principle employed for operational safety.

The external surface consists of a wooden board, externally layered by a hardened resin-impregnated layer. Penetration of this external layer is achieved by the nose-grinder rotating at high speed, driven by the high-torque brushless motor-tool. In this process, the UAS-control framework provides the stable basis required for consistent forceful application of the grinder-tool similarly to a technician's hand, maintaining a normal-to the surface pose via hor-

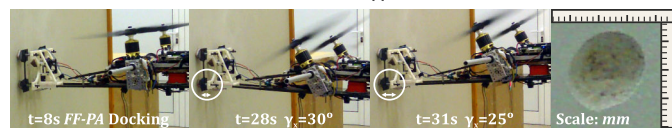
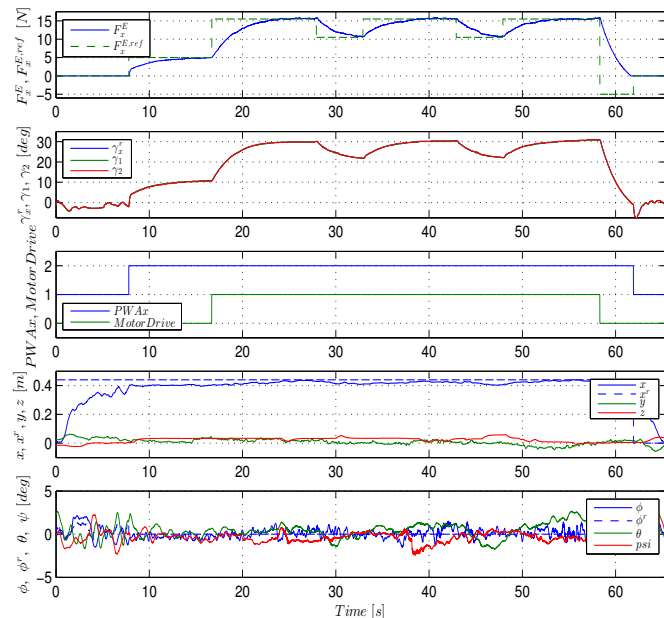


Fig. 6. Pulsating Force Control during Technical Activity

izontal hovering. Figure 5 illustrates the basic technical activity-execution maneuver, wherein the aforementioned principles can be validated in the presented results. It is notable that even after the initial contact, detected by the tactile switches and marked by the $PWA_x : 1 \rightarrow 2$ -transition, the x -position further increases with the F_x^E -applied force, owing to the compressible end-effector springs. Additionally, certain phases of the maneuver, documented in a video-sequence, are presented in image form.

Figure 6 demonstrates the capacity for force control, provided by the previously elaborated control structure, while performing a technical task. The presented maneuver consists of the same basic phases; it is however extended during the PA -phase by enacting a $F_x^{E,ref}$ pulsating force reference. The utility for such a function can be again intuitively understood via the human paradigm: while grinding a hole into a surface, a human operator would allow the excess removed material to escape in order to proceed in inner layers more effectively. This principle is implemented employing the compressible design of the end-effector, where the springs extend-or-compress based on the applied force. This receding-proceeding motion can be observed in the x -response. It is also noted that this experimental sequence resulted in a deeper-ground hole.

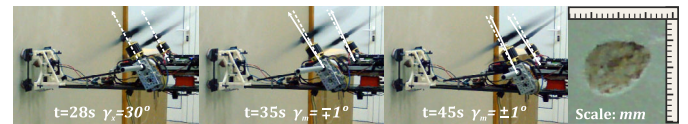
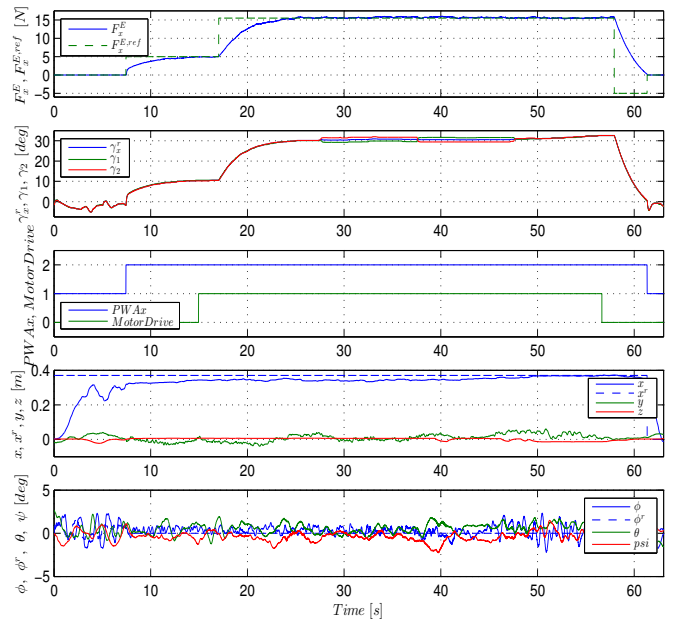


Fig. 7. Rotating-Moment Exertion for Side-Grinding

Figure 7 illustrates the successful implementation of the rotating moment-exertion principle (4) in technical tasks. One practical motivation for this utility is side-grinding: while exploiting the rotational flexibility of the end-effector design and the retained pitch control authority would allow side-grinding in the vertical direction, in order to perform side-grinding in the lateral direction requires a significant M_ψ^{VCP} moment to be generated. As noted, the principle of differential rotor-tilting can be exploited in order to achieve this, while no constant roll ϕ -disturbing moment

appears, as static equilibrium is obtained via concurrent differential rotor-thrusting. The effect of this operation can be readily observed by the end-result presented in the respective image sequence, via the laterally-elongated oval-shaped ground hole.

6. CONCLUSION

The application field of technical activities-execution with advanced UASs was addressed via the innovative exploitation of the directly-actuated thrust vectoring capabilities of an unmanned tiltrotor platform. The advantages of this approach were analyzed, while also justifying the specific design principles. A properly synthesized control scheme was implemented, based on a separately presented PWA modeling representation. The synthesized scheme relies on the principles of receding horizon optimal control, and provides a unified synthesis which efficiently handles: a) free-flight operation, b) surface docking/detaching, and c) technical activities execution via controlled forceful interaction. The resulting control scheme was evaluated in real-time execution. An important part of the controller's evaluation were the experimentally performed docking maneuvers, in order to initiate the technical tasks. Finally, various experimental sequences were conducted, evaluating the UAS's capacity for successful execution of technical tasks, while retaining operational safety.

REFERENCES

- K. Alexis, G. Nikolakopoulos, and A. Tzes. Model predictive quadrotor control: attitude, altitude and position experimental studies. *Control Theory & Applications, IET*, 12, volume 6:1812–1827, 2012.
- K. Alexis, G. Nikolakopoulos, and A. Tzes. Constrained-control of a quadrotor helicopter for trajectory tracking under wind-gust disturbances. *2010 IEEE Mediterranean Electrotechnical Conference (MELECON)*, 1411–1416, 2010.
- V. Goga, and P. Boek. Application of INS to mechatronic systems control and regulation using virtual dynamic models. *2013 IEEE International Conference on Process Control*, 185–189, 2013.
- D. Mellinger, Q. Lindsey, M. Shomin, and V. Kumar. Design, modeling, estimation and control for aerial grasping and manipulation. *2011 IEEE/RSJ International Conference on Intelligent Robots and Systems (IROS)*, 2668–2673, 2011.
- J. Thomas, J. Polin, K. Sreenath, and V. Kumar. Avian-inspired grasping for quadrotor micro UAVs. *2013 ASME International Design Engineering Technical Conferences (IDETC) and Computers and Information in Engineering Conference (CIE)*, 2013.
- P. Pounds, D. Bersak, and A. Dollar. The Yale aerial manipulator: grasping in flight. *2011 IEEE International Conference on Robotics and Automation (ICRA)*, 2974–2975, 2011.
- C. Korpela, M. Orsag, T. Danko, B. Kobe, C. McNeil, R. Pisch, P. Oh. Flight stability in aerial redundant manipulators. *2012 IEEE International Conference on Robotics and Automation (ICRA)*, 3529–3530, 2012.
- D. Mellinger, M. Shomin, N. Michael, and V. Kumar. Co-operative grasping and transport using multiple quadrotors. *Distributed Autonomous Robotic Systems*, 83:545–558, 2013.
- M. Manubens, D. Devaurs, and J. Cortes. Motion planning for 6d manipulation with aerial towedcable systems. *2013 IEEE Robotics Science and Systems Conference (RSS)*, 2013.
- K. Alexis, C. Huerzeler, and R. Siegwart. Hybrid modeling and control of a coaxial unmanned rotorcraft interacting with its environment through contact. *2013 IEEE International Conference on Robotics and Automation (ICRA)*, 5397–5404, 2013.
- G. Darivianakis, K. Alexis, M. Burri and R. Siegwart. Hybrid predictive control for aerial robotic physical interaction towards inspection operations. *2013 IEEE International Conference on Robotics and Automation (ICRA)*, to appear, 2014.
- B. Marconi and R. Naldi. Control of aerial robots: hybrid force and position feedback for a ducted fan. *IEEE Control Systems*, 4, volume 32:43–65, 2012.
- Y. Koveos, T. Kolyvas, L. Drikos. Robotic arm development for ultrasonic inspection. *2012 Computer and IT Applications in the Maritime Industries Conference (COMPIT)*, 258–268, 2012.
- C. Papachristos, K. Alexis, and A. Tzes. Model predictive hovering-translation control of an unmanned tri-tiltrotor. *2013 IEEE International Conference on Robotics and Automation (ICRA)*, 5404–5412, 2013.
- C. Papachristos, K. Alexis, and A. Tzes. Efficient force exertion for aerial robotic manipulation: exploiting the thrustvectoring authority of a tritiltrotor UAV. *2014 IEEE International Conference on Robotics and Automation (ICRA)*, to appear, 2014.
- C. Papachristos, K. Alexis, and A. Tzes. Towards a high-end unmanned tri-tiltrotor: design, modeling and hover control. *2012 IEEE Mediterranean Conference on Control Automation (MED)*, 1579–1584, 2012.
- C. Papachristos, K. Alexis, and A. Tzes. Design and experimental attitude control of an unmanned tiltrotor aerial vehicle. *2011 IEEE International Conference on Advanced Robotics (ICAR)*, 465–470, 2011.
- C. Papachristos, and A. Tzes. Large object pushing via a direct longitudinally-actuated unmanned tri-tiltrotor. *2013 IEEE Mediterranean Conference on Control Automation (MED)*, 173–178, 2013.
- L. Ljung. System identification: theory for the user. USA: Prentice Hall, Inc. (2nd Edition), 1999.
- J. Lofberg. Yalmip: A toolbox for modeling and optimization in MATLAB. *2004 IEEE Computer Aided Control System Design Conference (CACSD)*, 2004
- M. Herceg, M. Kvasnica, C. Jones, and M. Morari. Multi-parametric toolbox 3.0. *2013 European Control Conference (ECC)*, 502–510, 2013
- M. Kvasnica. Real-time model predictive control via multi-parametric programming: theory and tools. VDM Verlag, 2009
- M. Baotic. Optimal control of piecewise affine systems. Ph.D. Dissertation, Swiss Federal Institute of Technology Zurich, 2005
- A. Bemporad. Modeling, control, and reachability analysis of discrete-time hybrid systems. University of Sienna, 2003
- M. Kvasnica, I. Rauova, and M. Fikar. Yalmip: Automatic code generation for real-time implementation of model predictive control. *2010 IEEE Computer Aided Control System Design Conference (CACSD)*, 993–998, 2010